Title

Effect of block copolymer morphology controlled by casting-solvent quality on pervaporation of butanol/water mixtures

Authors

Shin, Chaeyoung
Chen, X Chelsea
Prausnitz, John M
et al.

Publication Date

2017-02-01

DOI

10.1016/j.memsci.2016.09.054

Peer reviewed

Journal of Membrane Science 523 (2017) 588–595

Contents lists available at ScienceDirect

Journal of Membrane Science

journal homepage: www.elsevier.com/locate/memsci

Effect of block copolymer morphology controlled by casting-solvent quality on pervaporation of butanol/water mixtures

Chaeyoung Shin[a,b], X. Chelsea Chen[a,b,c], John M. Prausnitz[a], Nitash P. Balsara[a,b,c,*]

[a] Department of Chemical and Biomolecular Engineering, University of California, Berkeley, CA 94720, USA
[b] Energy Biosciences Institute, University of California, Berkeley, CA 94704, USA
[c] Materials Sciences Division, Lawrence Berkeley National Laboratory, Berkeley, CA 94720, USA

ARTICLE INFO

Keywords:
Block copolymer morphology
Casting-solvent
Permeability
Pervaporation
Morphology factor

ABSTRACT

Motivated by the need for developing membranes for biofuel purification, we made pervaporation membranes by casting a polystyrene-*b*-polydimethylsiloxane-*b*-polystyrene (SDS) triblock copolymer using toluene, cyclohexane, and hexane as casting solvents. The three solvents have different affinities for each of the blocks of the SDS, which enables the creation of membranes with different nano-morphologies using the same block copolymer. These membranes were used in pervaporation experiments with butanol/water mixtures as the feed solution. We quantify the effect of morphology on butanol and water permeabilities. Poorly-ordered granular morphology, obtained from hexane-cast membranes, is optimal for selective butanol transport. Butanol permeability was a more sensitive function of morphology than water permeability. Butanol uptake measurements showed that morphology had negligible effects on solubility. Therefore, we attribute the dependence of permeability on morphology to differences in diffusivities.

1. Introduction

Production of biofuels by fermentation of biomass at an industrial scale continues to be a challenge. One of the challenges is product inhibition [1]. Product inhibition occurs at a relatively low biofuel concentration of 10–20 g/L, and results in the death of the fermentation microorganisms, thereby stopping any further biofuel production [2]. This limits the productivity and also results in high separation costs. Therefore, *in situ* product removal has become a topic of interest for many researchers [3]. Adsorption, liquid-liquid extraction, and pervaporation are some of the methods that researchers have tried to incorporate as means for *in situ* product removal [4–7].

Pervaporation is a membrane-based separation method which is advantageous because of its high product selectivity. The most widely used membrane material for the *in situ* removal of biofuel during fermentation is crosslinked polydimethylsiloxane (PDMS) [8–10]. An ideal membrane would be selectively permeable to the biofuels while withstanding the mechanical stresses necessary for operation. One approach for obtaining mechanically rigid membranes that are permeable is based on block copolymer self-assembly [11,12]. One of the blocks is designed to enable selective permeation while the other is generally impermeable but rigid, which enables control of mechanical properties. In a series of previous publications, we have studied permeation through polystyrene-*b*-polydimethylsiloxane-*b*-polystyrene (SDS) block copolymer membranes; polystyrene is a glassy and rigid polymer at room temperature, and functions as the mechanical block [13,14]. The selective permeation of biofuels through these membranes was better than that of commercial crosslinked PDMS membranes. Experiments wherein the biofuel (a mixture of butanol, acetone, and ethanol) produced by fermentation was removed by pervaporation through the SDS membrane showed better productivity than fermentation experiments with the crosslinked PDMS membrane [14].

It is well known that in bulk, block copolymers self-assemble into a variety of nano-scale equilibrium morphologies [15,16]. The equilibrium morphologies of block copolymers and solvents mixtures are affected by the selective solvation of individual blocks in the solvents [17,18]. When block copolymer membranes are made by solvent-casting, it is possible to trap non-equilibrium metastable states [19]. Previous studies of pervaporation through block copolymer membranes have focused on transport through equilibrium morphologies [20–22]. The geometries and sizes of the nanostructures were controlled by changing chain length and/or composition of the block copolymer. In this paper, we prepared films for pervaporation by casting block copolymer films from different solvents followed by thorough drying. A dilute mixture of butanol in water is used as a model solution for a biofuel fermentation broth, and was used as the

* Corresponding author at: Department of Chemical and Biomolecular Engineering, University of California, Berkeley, CA 94720, USA.
E-mail address: nbalsara@berkeley.edu (N.P. Balsara).

http://dx.doi.org/10.1016/j.memsci.2016.09.054
Received 27 May 2016; Received in revised form 1 September 2016; Accepted 12 September 2016
Available online 29 September 2016
0376-7388/

Nomenclature

ϕ_b	volume fraction of butanol in membrane
P_b	butanol permeability
P_w	water permeability
α_b	butanol selectivity
ϕ_{PDMS}	volume fraction of PDMS phase
P_i^0	permeability of i through pure PDMS
f_{Pi}	morphology factor associated with the permeability of i
K_i	solubility of i
D_i	diffusivity of i
c_i	molar concentration of i in the membrane
x_i	mole fraction of i in the liquid
γ_i	activity coefficient of i in the liquid
p_i^{sat}	saturated vapor pressure of i in the liquid
K_b^0	butanol solubility in pure PDMS
D_b^0	butanol diffusivity in pure PDMS
f_{Kb}	morphology factor associated with butanol solubility
f_{Db}	morphology factor associated with butanol diffusivity
$\chi_{b,p}$	Flory-Huggins parameter for the butanol-polymer system
Γ_b	butanol activity coefficient in the membrane based on volume fraction

feed solution in all pervaporation experiments. The same block copolymer was used in all experiments; thus, the nominal compositions of all the films are identical. We show that the solvent used for casting the membranes has a significant effect on selective permeation. Analysis of the morphology by small angle X-ray scattering and electron microscopy, along with butanol uptake experiments, are used to understand the underpinnings of these observations.

2. Experimental

2.1. Membrane preparation

A polystyrene-*b*-polydimethylsiloxane-*b*-polystyrene (SDS) triblock copolymer of molecular weight 22-104-22 kg/mol and polydispersity index of 1.3 was purchased from Polymer Source (Dorval, Canada). The chemical structure of the polymer is shown in Fig. 1. The polymer consists of 60 wt% SDS triblock copolymer, 30 wt% polystyrene-b-polydimethylsiloxane diblock copolymer of molecular weight 22–52 kg/mol, and 9 wt% homopolymer polystyrene (Viscotek GPC, Malvern). The polydimethylsiloxane (PDMS) volume fraction, determined by ^{1}H nuclear magnetic resonance (NMR) on toluene-d8 solutions, was 0.70. Using the nominal densities of PS and PDMS (1.04 and 0.970 g/cm^3) [23,24], the estimated PDMS volume fraction calculated using the block molecular weights supplied by Polymer Source is 0.72. Given the polydisperse nature of the sample, this difference is not surprising. Casting solvents, toluene, hexane, and cyclohexane, were purchased from Sigma Aldrich and were used as received.

1 g of SDS was dissolved into about 30 ml of the solvent of interest. The solution was then poured into a 3-in diameter Teflon petri dish. The dish was lightly covered with aluminum foil and a glass beaker. The solution was dried for 3–4 days. Afterward, the Teflon dish was placed in a vacuum chamber for one day to ensure the absence of any remaining solvent in the membrane. The absence of remaining solvent was checked by dissolving the membrane in a deuterated solvent that was different from the casting solvent and conducting NMR experiments to confirm the absence of the casting solvent. After the drying step, non-porous, free-standing membranes with thicknesses ranging from 100 to 150 μm were obtained.

2.2. Scanning transmission electron microscopy

To prepare scanning transmission electron microscopy (STEM) samples, a piece of the bulk membrane was mounted onto a cryomicrotome (Leica FC6) and cooled to −140~−120 °C. Thin sections with thicknesses of approximately 80 nm were obtained and transferred onto a lacey carbon-coated copper grid (Electron Microscopy Sciences). STEM was done on a Tecnai F20 UT FEG instrument using a high angle annular dark field detector (HAADF) with an acceleration voltage of 200 keV. The samples were not stained. The contrast of the images is resulted from the z-contrast between the silicon of the PDMS phase and the carbon of the PS phase.

2.3. Small angle X-ray scattering

Small angle X-ray scattering (SAXS) experiments were conducted at the Advanced Light Source (Lawrence Berkeley National Lab, Berkeley) from beamline 7.3.3. The sample-to-detector distance was 4 m, and the X-ray energy was 10 keV. Exposure time was 30 s for each sample. The collected 2D image was then azimuthally averaged and X-ray intensity was plotted as functions of the magnitude of the scattering wave vector, q, which is defined as $q=4\pi \sin(\theta/2)/\lambda$, where θ is the scattering angle and λ is the wavelength of the X-ray.

2.4. Butanol uptake measurement

Three membrane pieces were cut from the three different membranes: toluene-cast, cyclohexan-cast, and hexane-cast. The weight of the pieces ranged from 0.01 g to 0.1 g, and the thickness of the membranes were 100–150 μm. Each piece was placed in a 5 ml vial containing 1-butanol. All of the membrane samples were insoluble in butanol. The vials containing the membrane samples were placed in an oil bath at temperatures of interest. The vials were kept for about 24 h at each of the temperatures before the membrane samples were taken out and measured. The samples taken out of the butanol were dapped dry with paper towels before measuring the mass of the swollen samples. The ratio of the mass of the swollen membrane to that of the dry membrane is defined as butanol uptake. The butanol uptake was used to calculate the volume fraction of butanol in the membrane, ϕ_b, using pure component densities (butanol: 0.81 g/cm^3 [25], PS: 1.05 g/cm^3, PDMS: 0.96 g/cm^3 [26]) and neglecting volume change on mixing. (We attempted to measure water uptake and found that it was negligible.)

2.5. Pervaporation

Aqueous 1 wt% 1-butanol solution was used as feed for all of the pervaporation experiments. The butanol was purchased from Sigma Aldrich and was used as received. The pervaporation experiments were performed on a benchtop pervaporation unit purchased from Sulzer

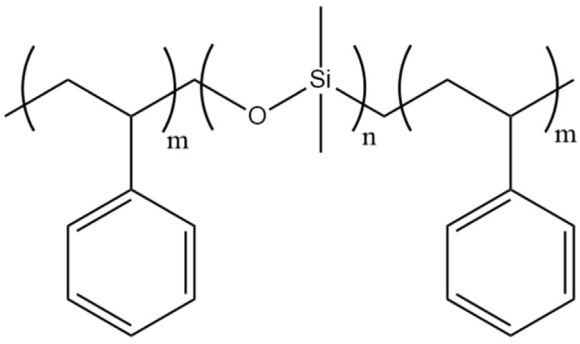

Fig. 1. Chemical structure of polystyrene-*b*-polydimethylsiloxane-*b*-polystrene triblock copolymer.

Chemtech as described in Ref. [13]. The collected permeate was analyzed by high performance chromatography (Prominence UFLC instrument, Shimadzu). The pervaporation experiments were repeated on 2–3 membranes. The data reported in this paper were obtained from the same membrane that was used in the uptake measurements. The pervaporation experiments using this membrane were run four times. We report the average value and take the standard deviation as a measure of experimental uncertainty.

2.6. Permeability and diffusivity

Permeabilities of butanol and water (P_b and P_w) through the membranes were calculated from data obtained from pervaporation experiments using methods described in Ref. [13]. Membrane selectivity relative to butanol (α_b) is defined as

$$\alpha_b = P_b/P_w \quad (1)$$

Following previous studies [13], we assume that butanol diffuses only through the PDMS phase of the membrane. Thus, permeability through block copolymer membranes is given by

$$P_i = f_{P_i}\,\phi_{PDMS}\,P_i^0 \ (i = \text{b or w}) \quad (2)$$

where ϕ_{PDMS} is the volume fraction of PDMS in the block copolymer (0.70), P_i^0 is the intrinsic permeability of species i through pure PDMS, and f_{Pi} is a morphology factor that accounts for geometric constraints on permeability.

For a dilute solution of butanol, P_i is expressed as [27]

$$P_i = K_i \times D_i \quad (3)$$

where K_i is the solubility of i and D_i is the diffusivity of i. K_i was obtained by equilibrating liquid butanol with the block copolymer membrane. In general,

$$K_i = \frac{c_i}{x_i \gamma_i p_i^{sat}} \quad (4)$$

where c_i is the molar concentration of i in the membrane, x_i is the mole fraction of i in the liquid, γ_i is the activity coefficient of i in the liquid, and p_i^{sat} is the saturated vapor pressure of i in the liquid [28,29]. For an aqueous 1 wt% butanol solution, x_b=0.0024.

Focusing on butanol permeability, we define K_b^0 and D_b^0 to be solubility and diffusivity of butanol in pure PDMS. Rewriting Eq. (3) in terms of these parameters, we obtain

$$P_b = f_{P_b}\,\phi_{PDMS}\,(K_b^0 \bullet D_b^0) \quad (5)$$

In principle, f_{Pb} can be separated into a morphology factor affecting sorption (f_{Kb}) and a morphology factor affecting diffusion (f_{Db}):

$$f_{P_b} = f_{K_b} \bullet f_{D_b} \quad (6)$$

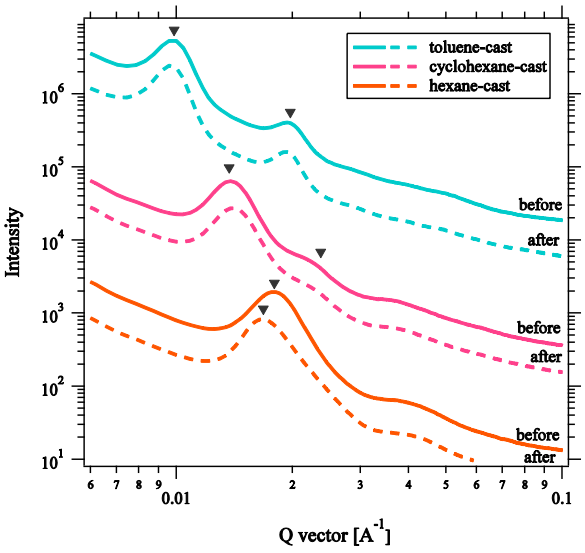

Fig. 2. Small angle X-ray scattering (SAXS) intensity as a function of the magnitude of the scattering Q vector for the toluene-cast, the cyclohexane-cast, and the hexane-cast membranes. Each of the solid curves represents the SAXS profile before the membrane was used in pervaporation experiments. The dotted curves represent the SAXS profiles after the membranes were used in pervaporation experiments. ▼ denotes the positions of the primary and secondary peaks.

Eq. (5) becomes

$$P_b = f_{K_b}\,K_b^0 \bullet f_{D_b}\,\phi_{PDMS}\,D_b^0 \quad (7)$$

where

$$K_b = f_{K_b}\,K_b^0 \quad (8)$$

and

$$D_b = f_{D_b}\,D_b^0 \quad (9)$$

Based on usual definitions of morphology factors [20,30], we expect diffusion to be affected by morphology but not solubility, i.e., we expect f_{Kb} to be unity and f_{Pb}=f_{Db}.

To obtain information on the thermodynamic properties of the butanol-polymer system, that is, to find the Flory-Huggins parameter $\chi_{b,p}$, we measured the butanol uptake for a membrane equilibrated in pure butanol. In this case,

$$\gamma_b x_b = 1 = \Gamma_b \phi_b \quad (10)$$

where Γ_b is the activity coefficient of butanol in the membrane based on volume fraction and ϕ_b is the volume fraction of butanol in the membrane. Using Flory-Huggins theory for mixtures of a high mole-

Table 1
Measured ϕ_b in 100% butanol, Γ_b in 100% butanol, $\chi_{b,p}$, γ_b in aqueous 1% butanol, calculated ϕ_b in aqueous 1% butanol, and Γ_b in aqueous 1% butanol for the three membranes at different temperatures.

Casting solvent	Temperature (°C)	Measured ϕ_b (100% butanol)	Γ_b (100% butanol)	$\chi_{b,p}$	γ_b (1% butanol)	Calculated ϕ_b (1% butanol)	Γ_b (1% butanol)
Toluene	37	0.217	4.60	1.21	43.3	0.0118	8.79
	50	0.333	3.00	0.983	43.2	0.0151	6.88
	60	0.371	2.69	0.916	42.7	0.0158	6.50
	80	0.568	1.76	0.716	35.7	0.0160	5.35
Cyclohexane	37	0.290	3.45	1.05	43.3	0.0140	7.42
	50	0.357	2.80	0.936	43.2	0.0156	6.63
	60	0.413	2.42	0.863	42.7	0.0167	6.16
	80	0.597	1.68	0.695	35.7	0.0163	5.24
Hexane	37	0.277	3.60	1.07	43.3	0.0137	7.61
	50	0.336	2.98	0.968	43.2	0.0151	6.85
	60	0.414	2.41	0.861	42.7	0.0167	6.15
	80	0.598	1.67	0.694	35.7	0.0164	5.24

γ_b taken from Ref. [32].

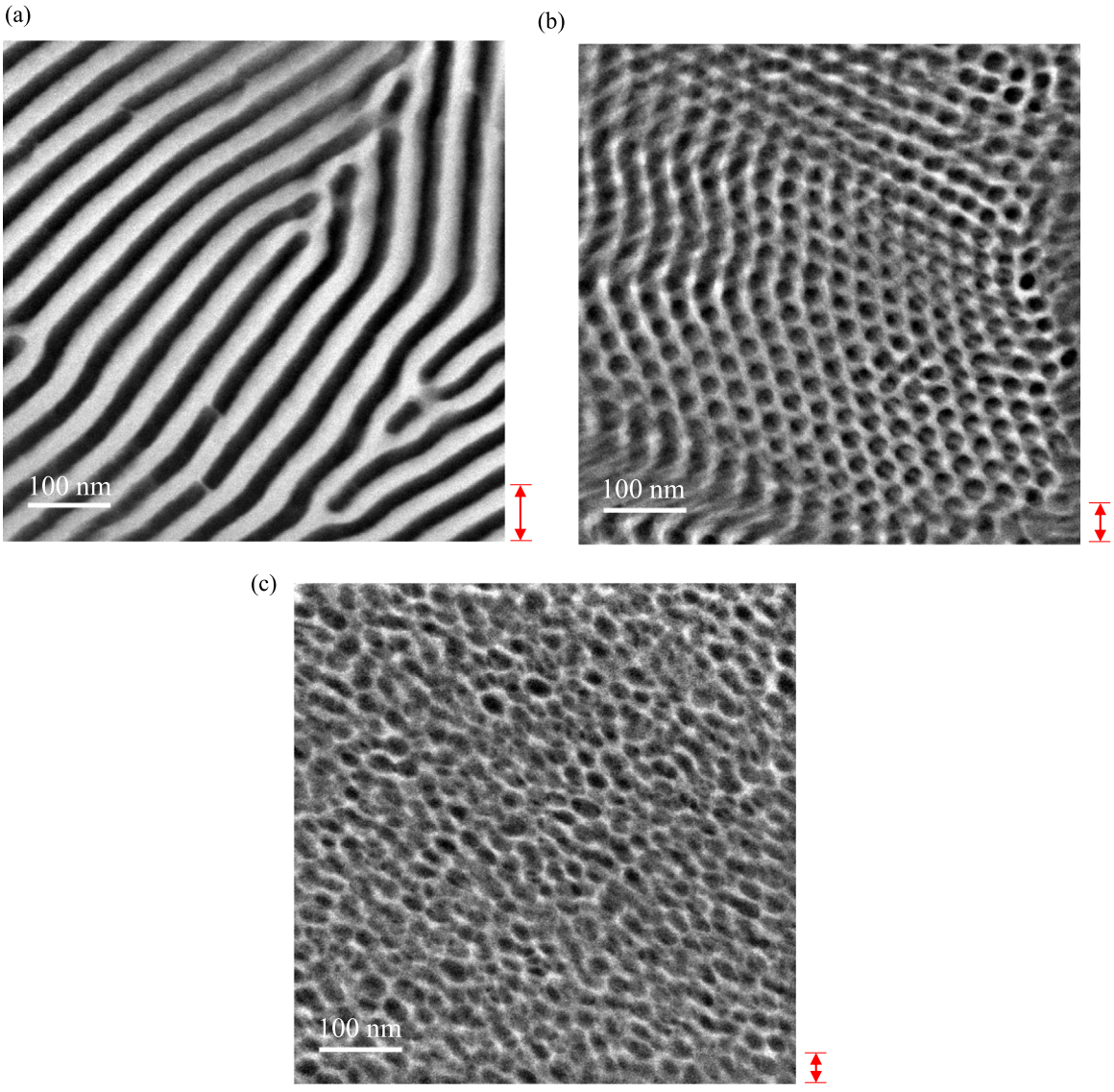

Fig. 3. Dark-field scanning transmission electron microscopy (STEM) images of the (a) toluene-cast, (b) cyclohexane-cast, and (c) hexane-cast membranes. The brighter phase is the PDMS-rich phase, and the darker phase is the PS-rich phase. The white scale bar represents 100 nm. All of the images were taken at the same magnification. The red arrows represent the domain sizes calculated from SAXS.

cular-weight homopolymer and solvent [31]

$$ln\Gamma_b=1-\phi_b+\chi_{b,p}(1-\phi_b)^2 \quad (11)$$

Using Eq. (10), pure butanol uptake measurements enabled determination of $\chi_{b,p}$. Table 1 shows results obtained for the three membranes.

The volume fraction of butanol in the membrane equilibrated in the pervaporation feed solution (1 wt% butanol) is then estimated using $\chi_{b,p}$.

$$\gamma_b x_b=\Gamma_b\phi_b \quad (12)$$

noting that the γ_b and x_b now refer to the feed solution. γ_b at each temperature was estimated using the non-random two-liquid (NRTL) equation for binary butanol-water mixtures [32]. For temperatures between the data provided in Ref. [32], linear extrapolation was used to estimate γ_b.

3. Results and discussion

The three solvents chosen for casting the membranes exhibit varying affinities for the blocks of the polystyrene-*b*-polydimethylsiloxane-*b*-polystyrene (SDS) block copolymer. Toluene dissolves both blocks, cyclohexane is a theta solvent for polystyrene (PS) and a good solvent for polydimethylsiloxane (PDMS), and hexane is a poor solvent for PS and a good solvent for PDMS. Using the three different solvents for solvent-casting resulted in drastically different morphologies.

In Fig. 2, we show SAXS profiles of membranes cast from different solvents before they were used in pervaporation experiments and after completing the experiments. All of the profiles exhibit a well-defined primary scattering peak at scattering vector $q=q^*$. This indicates the presence of periodic structures with domain spacings $d=2\pi/q^*$. The domain spacing represents the average center-to-center distance between adjacent PDMS microdomains. The domain spacings for membranes cast from toluene, cyclohexane, and hexane are 65.3 nm, 45.7 nm, and 35.2 nm, respectively. The domain spacing decreases with decreasing solvent quality. A higher order scattering peak at $q=2q^*$ is seen in the toluene-cast membrane, indicating lamellar morphology. In the case of the cyclohexane-cast membrane, a shoulder is seen at $q=\sqrt{3}q^*$, suggesting a cylindrical morphology. The scattering profiles obtained before and after pervaporation are nearly identical. The largest difference is seen in the hexane-cast membrane wherein the domain spacing changes from 35.2 nm to 37.4 nm. It is evident that the

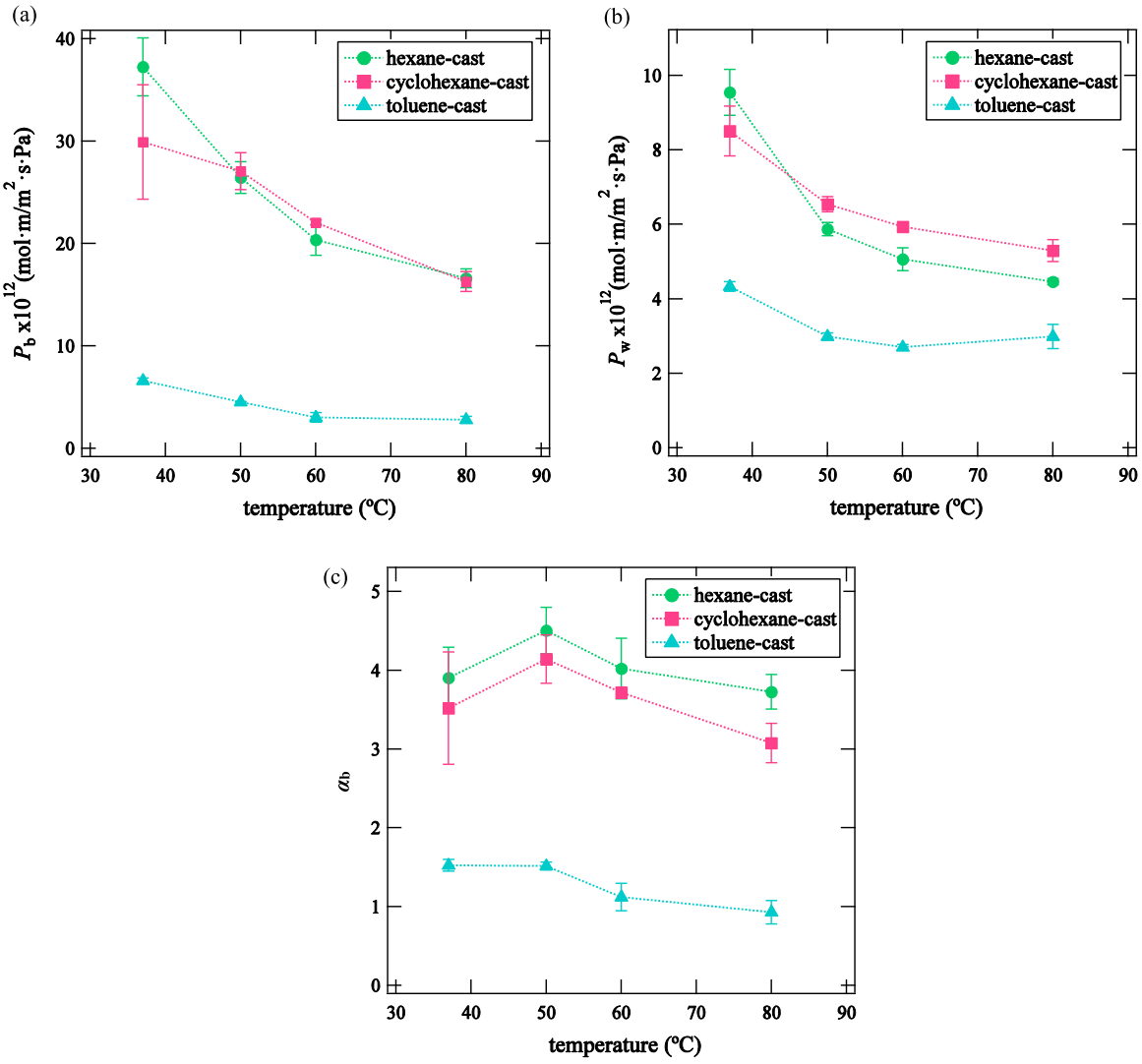

Fig. 4. Butanol-water binary component pervaporation results at 37, 50, 60, and 80 °C. (a) Butanol permeabilities (P_b), (b) water permeabilities (P_w), and (c) butanol selectivities (α_b) are plotted as functions of temperatures for the hexane-cast (●), the cyclohexane-cast (■), and the toluene-cast (▲) membranes.

Table 2
Vapor pressure for pure butanol (p_b^{sat}) and concentration of butanol in membrane (c_b) for the three membranes at different temperatures.

Temperature (°C)	p_b^{sat}	c_b (mol/m^3)		
	(mmHg)	Toluene-cast	Cyclohexane-cast	Hexane-cast
37	15.0	129	153	149
50	33.6	165	171	165
60	59.2	172	182	182
80	162.3	175	179	179

p_b^{sat} taken from Ref. [29].

membrane morphologies are effectively trapped during the pervaporation experiments.

Further confirmation of the different morphologies was made by scanning transmission electron microscopy (STEM). Fig. 3 shows the STEM images of toluene-cast, cyclohexane-cast, and hexane-cast membranes. The toluene-cast membrane has lamellar morphology, cyclohexane-cast membrane has cylindrical morphology with PS cylinders, and the hexane-cast membrane has a poorly-ordered granular morphology with dark PS domains in a bright PDMS matrix. The equilibrium morphology of the block copolymer is expected to be cylindrical based on the fact that the PDMS volume fraction is 0.70. It is evident that the morphologies of our block copolymer membranes depend on interactions between the blocks and the solvent, [17,18] and perhaps other parameters such as evaporation rates. The domain spacings observed by STEM are consistent with the domain spacings calculated from the SAXS profiles; the SAXS domain spacings are represented by by red arrows in Fig. 3.

The butanol permeabilities (P_b) and water permeabilities (P_w) of the three membranes were measured by pervaporation experiments using aqueous 1 wt% butanol solutions as feed. Permeabilities were determined at different temperatures: 37, 50, 60, and 80 °C. P_b and P_w are plotted as functions of temperature in Fig. 4a and b, respectively. P_b and P_w of the three membranes decreased monotonically as the pervaporation temperature was increased. This is consistent with

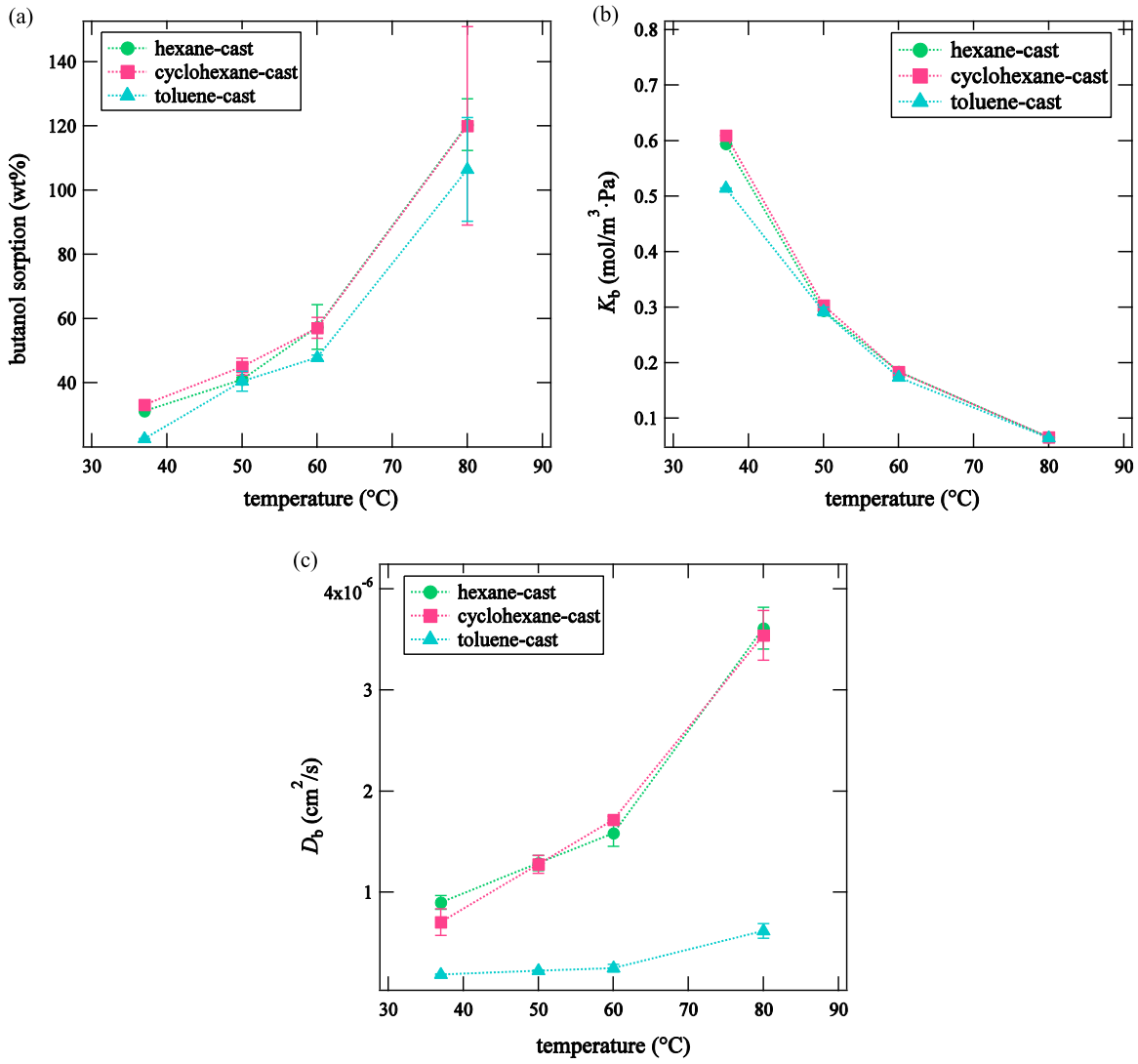

Fig. 5. (a) Butanol uptake, (b) butanol solubility (K_b), and (c) butanol diffusivity (D_b) as functions of temperature in hexane-cast(●), cyclohexane-cast(■), and toluene-cast(▲) membranes.

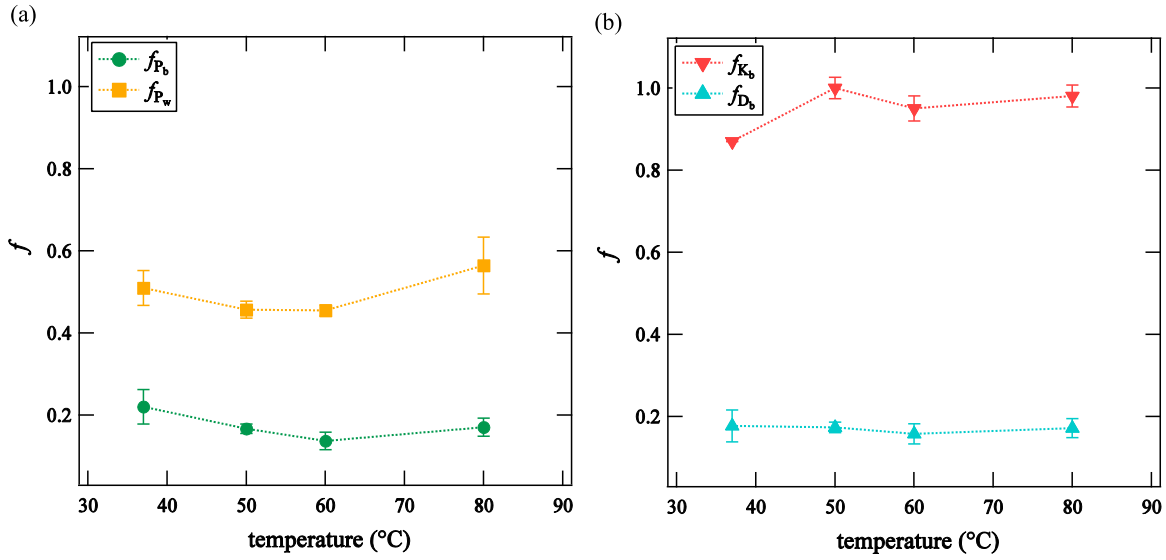

Fig. 6. (a) Morphology factor associated with butanol permeability (f_{Pb}) (●) and morphology factor associated with water permeability (f_{Pw}) (○), (b) morphology factor associated with butanol solubility (f_{Kb}) (▼) and morphology factor associated with butanol diffusivity (f_{Db}) (▲) of the toluene-cast membrane as functions of temperature.

literature [33]. (Both butanol and water fluxes increase with temperature due to an increase in the driving forces for pervaporation, see p_b^{sat} in Table 2.) The hexane-cast and cyclohexane-cast membranes showed similar P_b and P_w at all temperatures. P_b obtained from these two membranes are within experimental error, while small differences outside the experimental error are seen in P_w. The toluene-cast membrane has the lowest P_b and P_w across all temperatures. P_b of the toluene-cast membrane are about 20 % of those of the hexane-cast and cyclohexane-cast membranes, and P_w of the toluene-cast membrane are about 50 % of those of the other membranes. Fig. 4c is a plot of the butanol selectivities (α_b) of the three membranes versus temperature. α_b is insensitive to temperature. α_b for the hexane- and cyclohexane-cast membranes are about 3.8 while that of the toluene-cast membrane is 1.3.

In attempt to explain the differences in P_b, P_w, and α_b, apparent PDMS volume fractions were derived from the STEM images. Although the same SDS was used to cast all three membranes, we did not want to disregard the possibility of non-equilibrium effects. The PDMS volume fractions were measured to be 0.52 and 0.54 for the toluene-cast membrane and the cyclohexane-cast membrane, respectively. (We did not attempt to estimate PDMS volume fraction for the hexane-cast membrane.) These numbers are different from the PDMS volume fraction determined by NMR, 0.70. It appears that the PDMS volume fraction determined by STEM is consistently lower than that determined by NMR. We are not sure about the reason for this difference. It may be related to STEM sample preparation.

Butanol uptake measurements were conducted to estimate butanol solubility in the three membranes. Fig. 5a shows results of uptake experiments measured by immersing the membranes in pure butanol. These butanol uptake measurements were used to calculate the volume fraction of butanol in the membrane, ϕ_b, using pure component densities as described experimental section. ϕ_b for the three membrane are listed in Table 1. This enables calculation of Γ_b for pure butanol using Eq. (10), and $\chi_{b,p}$ using Eq. (11). Assuming $\chi_{b,p}$ is independent of butanol concentration, we then simultaneously solve Eqs. (11) and (12) to determine Γ_b and ϕ_b for an aqueous 1 wt% butanol solution, using γ_b from literature [32] for the aqueous 1 wt% butanol solution. The measured ϕ_b and Γ_b for pure butanol, $\chi_{b,p}$, and γ_b, calculated ϕ_b, and Γ_b for the aqueous 1 wt% butanol solution at different temperatures for the three membranes are given in Table 1.

In Table 2, we give the temperature dependence of p_b^{sat} and c_b of the three membranes. This information, along with γ_b in Table 1, is used to calculate K_b for each membrane using Eq. (4). The temperature dependence of K_b in three membranes is shown in Fig. 5b. While butanol uptake and c_b increases significantly with increasing temperature, K_b decreases with temperature due to the temperature dependence of the other parameters in Eq. (4). The butanol uptake and K_b of the membranes do not depend on the solvent used for casting the membranes (Fig. 4a and b). Differences in P_b seen in Fig. 4a thus cannot be attributed to differences in solubility, K_b. The solubility measurements, however, provide an explanation for the decrease in butanol permeability with increasing temperature.

From P_b and K_b, butanol diffusivities (D_b) were calculated using Eq. (3) and plotted as functions of temperature (Fig. 5c). As expected, D_b increases monotonically with increasing temperature for all three membranes. The toluene-cast membranes exhibited the lowest D_b at all temperatures, while the hexane-cast membrane and the cyclohexane-cast membrane exhibited similar D_b at all temperatures because both P_b and K_b are similar. For comparison, D_b in aqueous 1 wt% butanol solution at 25 °C has been reported in literature to be 9.2×10^{-6} cm^2/s [34]. D_b in the membranes measured at 37 °C were about an order of magnitude smaller; they were calculated to be 1.2×10^{-7} cm^2/s, 5.1×10^{-7} cm^2/s, and 6.6×10^{-7} cm^2/s, respectively for toluene-cast, cyclohexane-cast, and hexane-cast membranes.

We use the framework described in the experimental section (Eqs. (2)–(9)) to study the effect of morphology on permeation. In this framework, the morphology factor (f) accounts for the microphase-separated geometry of the block copolymer. For lamellar morphologies, f = 2/3, while for morphologies with continuous transporting phases, f=1 [20,30]. In both cyclohexane- and hexane-cast membranes, the transporting PDMS-rich microphase is continuous and we thus expect f=1 in these systems. By definition, neither ϕ_{PDMS} nor P_i^0 are affected by the casting solvent. Our framework thus predicts that butanol and water permeabilities through cyclohexane- and hexane-cast membranes should be within experimental error. Our measurements are more-or-less consistent with this prediction (Fig. 4). Our framework also enables analysis of permeation through toluene-cast membranes. We estimate P_i^0 using data obtained from the hexane-cast membrane assuming that f_{Pi}=1. P_i^0 thus obtained are thus a factor of 1/0.70 larger than the butanol and water permeabilities of the hexane-cast membranes in Fig. 3a and b. Using P_i^0, we determine f_{Pi} for the toluene-cast membrane with lamellar morphology. Fig. 6a shows the results obtained. Both f_{Pw} and f_{Pb} are more-or-less independent of temperature. The average value of f_{Pw} is 0.50, which is somewhat lower than the expected value of 0.67. This suggests that defects in the lamellar phase slow down transport of water molecules. It is not uncommon to obtain morphology factors that are lower than theoretical limits [35,36]. What is surprising, however, is that f_{Pb} is about a factor of three smaller than f_{Pw}. The fact that water permeability is unaffected by morphology suggests that water molecules may be permeating through both PS- and PDMS-rich microphases.

Since permeability depends on solubility and diffusivity, f_{Pb} can, in principle, be affected by both parameters. This is explicitly quantified in Eq. (6). The morphology factor related to solubility, f_{Kb}, for the toluene-cast membrane, is estimated from measurements of K_b in toluene- and hexane-cast membranes in a manner that is analogous to our determination of f_{Pb} for the toluene-cast membrane. From Eq. (8), it is evident that f_{Kb} is given by the ratio $K_{b,toluene}/K_{b,hexane}$. In Fig. 6b, we plot f_{Kb} versus temperature. The morphology factor associated with diffusivity is then given by $f_{Db}=f_{Pb}/f_{Kb}$ (see Eqs. (3)–(9)). In Fig. 6b, we also plot f_{Db} versus temperature. It is evident that both f_{Kb} and f_{Db} are independent of temperature. To a good approximation f_{Kb} is unity (average value 0.95) while f_{Db} is about 0.17. This indicates that morphology affects diffusivity, not solubility. We hypothesize that defects such as T-junctions are responsible for hindering butanol transport through the toluene-cast lamellar SDS membrane. Further work is needed to either prove or disprove this hypothesis.

4. Conclusions

We used toluene, cyclohexane, and hexane, which have varying affinities for each of the blocks in SDS, as solvents for casting pervaporation membranes. The difference in the casting solvents resulted in different morphologies: the toluene-cast membrane exhibited a lamellar morphology, the cyclohexane-cast membrane exhibited a cylindrical morphology with a PDMS-rich matrix, and the hexane-cast membrane exhibited a poorly-ordered granular morphology with a PDMS-rich matrix (Figs. 1 and 2). These membranes were used in pervaporation experiments with an aqueous butanol solution as the feed. This enabled quantification of butanol and water permeabilities (Fig. 4). We expect permeability to be largely restricted to the PDMS-rich microphase. Since all of the membrane have the same composition, our experiments thus provide a unique window into the effect of morphology on simultaneous transport of butanol and water. The poorly-ordered granular morphology is optimal for selective butanol transport. Surprisingly, butanol permeability is more strongly affected by morphology than water permeability (Fig. 6a). Butanol uptake measurements showed that morphology had negligible effect on solubility (Fig. 6b). The observed dependence of permeability on morphology is thus attributed to differences in diffusivities.

It is evident that the choice of solvent used for casting block copolymer membranes can have a large effect on membrane perme-

ability. Further work is needed to elucidate the relationship between block copolymer processing, morphologies of block copolymer membranes, and transport mechanisms of mixtures of molecules through block copolymer membranes.

Acknowledgements

This work was supported by the Energy Biosciences Institute, University of California at Berkeley (Grant number OO3J04).

References

[1] B. Maiorella, H.W. Blanch, C.R. Wilke, By-product inhibition effects on ethanolic fermentation by saccharomyces cerevisiae, Biotechnol. Bioeng. 25 (1) (1983) 103–121.
[2] I. Maddox, N. Qureshi, K. Roberts-Thomson, Production of acetone-butanol-ethanol from concentrated substrate using clostridium acetobutylicum in an integrated fermentation-product removal process, Process Biochem. 30 (3) (1995) 209–215.
[3] J.M. Woodley, et al., Future directions for in-situ product removal (ISPR), J. Chem. Technol. Biotechnol. 83 (2) (2008) 121–123.
[4] N. Qureshi, et al., Energy-efficient recovery of butanol from model solutions and fermentation broth by adsorption, Bioprocess. Biosyst. Eng. 27 (4) (2005) 215–222.
[5] M. Minier, G. Goma, Ethanol production by extractive fermentation, Biotechnol. Bioeng. 24 (7) (1982) 1565–1579.
[6] D. O'Brien, J. Craig Jr, Ethanol production in a continuous fermentation/membrane pervaporation system, Appl. Microbiol. Biotechnol. 44 (6) (1996) 699–704.
[7] L.M. Vane, Separation technologies for the recovery and dehydration of alcohols from fermentation broths, Biofuels Bioprod. Biorefin. 2 (6) (2008) 553–588.
[8] L.M. Vane, A review of pervaporation for product recovery from biomass fermentation processes, J. Chem. Technol. Biotechnol. 80 (6) (2005) 603–629.
[9] G. Liu, et al., Pervaporation performance of PDMS/ceramic composite membrane in acetone butanol ethanol (ABE) fermentation–PV coupled process, J. Membr. Sci. 373 (1–2) (2011) 121–129.
[10] T. Mohammadi, A. Aroujalian, A. Bakhshi, Pervaporation of dilute alcoholic mixtures using PDMS membrane, Chem. Eng. Sci. 60 (7) (2005) 1875–1880.
[11] K.-i Okamoto, et al., Pervaporation of water-ethanol mixtures through poly-dimethylsiloxane block-copolymer membranes, Polym. J. 19 (6) (1987) 747–756.
[12] D.-G. Kim, et al., Hydroxyhexafluoroisopropylnorbornene block and random copolymers via vinyl addition polymerization and their application as biobutanol pervaporation membranes, Chem. Mater. 27 (19) (2015) 6791–6801.
[13] A.E. Ozcam, et al., Relationship between segregation strength and permeability of ethanol/water mixtures through block copolymer membranes, Macromolecules 46 (24) (2013) 9652–9658.
[14] C. Shin, et al., Block copolymer pervaporation membrane for in situ product removal during acetone–butanol–ethanol fermentation, J. Membr. Sci. 484 (2015) 57–63.
[15] F.S. Bates, G.H. Fredrickson, Block copolymer thermodynamics: theory and experiment, Annu. Rev. Phys. Chem. 41 (1) (1990) 525–557.
[16] Y. Mai, A. Eisenberg, Self-assembly of block copolymers, Chem. Soc. Rev. 41 (18) (2012) 5969–5985.
[17] T. Inoue, et al., Thermodynamic interpretation of domain structure in solvent-cast films of A–B type block copolymers of styrene and isoprene, J. Polym. Sci. Part A-2: Polym. Phys. 7 (8) (1969) 1283–1301.
[18] T.P. Lodge, B. Pudil, K.J. Hanley, The full phase behavior for block copolymers in solvents of varying selectivity, Macromolecules 35 (12) (2002) 4707–4717.
[19] J.C. Saam, F.G. Fearon, Properties of polystyrene-polydimethylsiloxane block copolymers, Ind. Eng. Chem. Prod. Res. Dev. 10 (1) (1971) 10–14.
[20] D.J. Kinning, E.L. Thomas, J.M. Ottino, Effect of morphology on the transport of gases in block copolymers, Macromolecules 20 (5) (1987) 1129–1133.
[21] Y.A. Elabd, C.W. Walker, F.L. Beyer, Triblock copolymer ionomer membranes, J. Membr. Sci. 231 (1–2) (2004) 181–188.
[22] T. Miyata, S. Obata, T. Uragami, Morphological effects of microphase separation on the permselectivity for aqueous ethanol solutions of block and graft copolymer membranes containing poly (dimethylsiloxane), Macromolecules 32 (11) (1999) 3712–3720.
[23] C.A. Finch, Polymer Handbook, 3rd ed., in: J. Brandrup and E.H. Immergut (Eds.), Wiley-Interscience, Chichester, 1989.
[24] O.K. Bates, Thermal conductivity of liquid silicones, Ind. Eng. Chem. 41 (9) (1949) 1966–1968.
[25] F. Alaoui, et al., Liquid density of 1-butanol at pressures up to 140 MPa and from 293.15 K to 403.15 K, Fluid Phase Equilib. 301 (2) (2011) 131–136.
[26] B. Ellis, R. Smith, Polymers: A Property Database, Second Edition, CRC Press, Boca Raton, Florida, 2008.
[27] J. Wijmans, R. Baker, The solution-diffusion model: a review, J. Membr. Sci. 107 (1) (1995) 1–21.
[28] R.W. Baker, J.G. Wijmans, Y. Huang, Permeability, permeance and selectivity: a preferred way of reporting pervaporation performance data, J. Membr. Sci. 348 (1–2) (2010) 346–352.
[29] J. Gmehling, et al., Vapor-Liquid Equilibrium Data Collection (Chemistry Data Series) I, Dechema, Flushing, NY, 1977.
[30] J. Sax, J. Ottino, Modeling of transport of small molecules in polymer blends: application of effective medium theory, Polym. Eng. Sci. 23 (3) (1983) 165–176.
[31] M. Doi, Introduction to Polymer Physics, Clarendon Press, Oxford, 1996.
[32] J.M. Sorensen, W. Arlt, Liquid-Liquid Equilibrium Data Collection (Chemical Data Series) V, Dechema, Frankfurt/Main, 1979.
[33] D.R. Greer, A.E. Ozcam, N.P. Balsara, Pervaporation of organic compounds from aqueous mixtures using polydimethylsiloxane-containing block copolymer membranes, AIChE J. 61 (9) (2015) 2789–2794.
[34] P.A. Lyons, C.L. Sandquist, A study of the diffusion of n-butyl alcohol in water using the Gouy interference method, J. Am. Chem. Soc. 75 (16) (1953) 3896–3899.
[35] I. Villaluenga, et al., Nanoparticle-driven assembly of highly conducting hybrid block copolymer electrolytes, Macromolecules 48 (2) (2015) 358–364.
[36] R.L. Weber, et al., Effect of nanoscale morphology on the conductivity of polymerized ionic liquid block copolymers, Macromolecules 44 (14) (2011) 5727–5735.